Response of Cylindrical Composite Structures Subjected to Underwater Impulsive Loading: Experimentations and Computations

Tao Qu
The George W. Woodruff School of Mechanical Engineering,
Georgia Institute of Technology,
Atlanta, GA 30332

Siddharth Avachat
The George W. Woodruff School of Mechanical Engineering,
Georgia Institute of Technology,
Atlanta, GA 30332

Min Zhou[1]
Fellow ASME
The George W. Woodruff School of Mechanical Engineering,
Georgia Institute of Technology,
Atlanta, GA 30332
e-mail: min.zhou@gatech.edu

The dynamic response of both thick-walled and thin-walled cylindrical composite structures subjected to underwater impulsive loads is analyzed. In the case of thick-walled structures, a novel experimental setup, the underwater shock loading simulator (USLS), is used to generate the impulsive loads. Deflection and core compression are characterized using high-speed digital imaging. The experiments are supported by fully dynamic numerical calculations which account for fluid–structure interactions (FSIs) and damage and failure mechanisms in the materials. The analysis focuses on the effect of varying structural attributes and material properties on load-carrying capacity, deformation mechanisms, and damage. Results show that cylindrical sandwich structures have superior blast-resistance than cylindrical monolithic structures of equal mass with only relatively minor increases in wall thickness. In the case of thin-walled structures, a unique computational framework based on a coupled Eulerian–Lagrangian (CEL) approach is developed to study the structural collapse and damage evolution under large impulsive loads which induces an implosion event. Simulations are carried out for a range of hydrostatic pressure and impulsive load intensity, with different loading configurations. Ply level stress analysis provides an insight on the stress–structural deformation–damage evolution relationship during the severe explosion-induced implosion event. The experiments, computations, and structure–performance relations developed in the current study offer approaches for improving the blast-mitigation capabilities of cylindrical composite sections in critical parts of marine structures, such as the keel, hull, and pipes.
[DOI: 10.1115/1.4035767]

Keywords: underwater blast loading, implosion, fluid–structure interaction (FSI), coupled Eulerian–Lagrangian (CEL) formulation, cohesive finite element method (CFEM), composite structures, sandwich structures, dynamic deformation, failure

1 Introduction

Ships, submersibles, and other marine structures are susceptible to damage due to dynamic loading from underwater explosions, projectile impact, and hull slamming resulting from high-speed motion. In recent years, there has been increased interest in using composite materials, such as fiber-reinforced laminates and sandwich composites, for such marine structures to reduce weight, improve corrosion resistance, and achieve good blast mitigation. A major aspect of composite structures in underwater applications that has not been thoroughly investigated is the response of cylindrical structures to blast loads. Cylindrical sections are classified as thick-walled structures with small length-to-diameter ratios (L/D) and thin-walled structures with large L/D ratios. The primary failure mechanism for thick-walled, small L/D structures is ply failure including interlaminar delamination and intralaminar cracking [1]. Drop weight and impact indentation testing has been performed to understand the dynamic response and damage of glass fiber composite cylinders intended for underwater applications [2–7]. Gas gun based impact loading has been successfully used to generate impulsive loading through water [8–16]. Thin-walled, large L/D ratio structures are more likely to fail by dynamic instability [1]. One such condition is that of implosion [17–23]. Implosion is caused by quasi-static pressurization to the critical buckling pressure of the structure, i.e., hydrostatically induced implosion, or through a combination of subcritical pressures and an underwater explosive (UNDEX) loading, i.e., explosive-induced implosion [17,20]. Most recently, the implosion of carbon fiber composite tubes was studied experimentally within a novel pressure vessel filled with water using digital image correlation (DIC) to relate collapse mechanics to the changes in local pressure fields [18–22]. So far, most studies are limited to hydrostatically induced implosion, and the limited instrumentation in the tests does not include any direct measurement of the physical values, such as stress, strain, and energy, in an explosive-induced implosion event. Predictions capturing these mechanisms using numerical approaches that account for structural attributes and loading conditions are required. Recent developments in finite element models have focused on highly nonlinear FSI problems with the account of large deformations and self-contact [23–27]. One approach is to simulate the fluid with Eulerian meshes and the solid structure with Lagrangian meshes. This technique is termed the CEL framework and was validated against the experimental data of the implosion testing conducted with thin-wall aluminum tubes [23–26]. However, no computational work exists on explosive-induced implosions of composite cylinders, and earlier computational studies did not account for materials damage or evaluate collapse pressure.

[1]Corresponding author.

Contributed by the Materials Division of ASME for publication in the JOURNAL OF ENGINEERING MATERIALS AND TECHNOLOGY. Manuscript received June 15, 2016; final manuscript received January 10, 2017; published online February 9, 2017. Assoc. Editor: Xi Chen.

The objective of the present work is to characterize the dynamic deformation and damage response of both thick-walled and thin-walled composite cylindrical structures subjected to high-intensity underwater impulsive loads. To investigate the response of thick-walled structures with small *L*/*D* ratios, a novel experimental setup called the USLS [8–11] is developed and a complementary cohesive finite element method (CFEM) is employed to track the progressive damage process. To investigate the response of thin-walled structures with large *L*/*D* ratios, a three-dimensional (3D) finite element model is developed based on a CEL approach to investigate the various aspects of the implosion event. Simulations are carried out for a range of hydrostatic pressure and impulsive load intensity with different loading configurations. The analyses focus on the effect of varying structural attributes and loading intensities on deflection, collapse mode evolution, energy dissipation, and damage.

2 Experimental Setup

Planar underwater impulses are generated using a novel experimental setup in the USLS. The USLS consists of a projectile impact based impulsive loading mechanism and clamped and simply supported boundary conditions for the sample. The cylindrical structure is supported on a steel flange because this loading condition closely resembles that found in a naval structure. A force transducer is mounted on the flange to measure impulses transmitted in each case. The location of the failure modes in this configuration allows accurate time-resolved measurements using high-speed digital imaging. Specifically, high-speed digital imaging and digital image correlation enable the study of deflection, face wrinkling, core-face debonding, core compression, core shear cracking and rupture, and their dependence on load intensity and core characteristics. This experimental setup is shown in Fig. 1(*a*). The USLS can generate impulsive loads with peak pressures within the range of 40–250 MPa, which resemble those created by an underwater explosion. Figure 1(*b*) shows the pressure histories of underwater impulses corresponding to different projectile velocities.

3 Materials

The thick-walled, small *L*/*D* ratio composite specimens are constructed with glass fiber reinforced plastic with two winding angles [45 deg] and [−45 deg]. The wall thickness of monolithic cylindrical specimens is 5.5 mm, and the inner diameter is 80 mm. For the sandwich structure, the outer face is 3.5 mm thick, the inner face is 2.5 mm thick, and the sandwich core is 10 mm thick. The inner diameter of the sandwich cylinder is 80 mm. The core material is Divinycell HP100 polyvinyl chloride (PVC) foam manufactured by DIAB, Inc., DeSoto, TX [28]. The sandwich structure has the same mass as the monolithic structure with only slightly higher wall thickness. Figure 2 shows the different components of a filament-wound composite cylinder. The sandwich

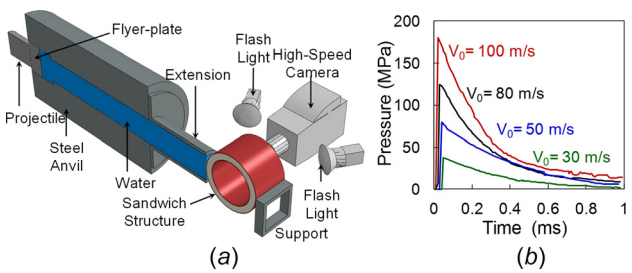

Fig. 1 (*a*) Sectional view of underwater shock loading simulator showing the setup for high-speed digital imaging and digital image correlation of impulsively loaded cylindrical sandwich structures and (*b*) measured experimental pressure histories in the water chamber for four different projectile velocities

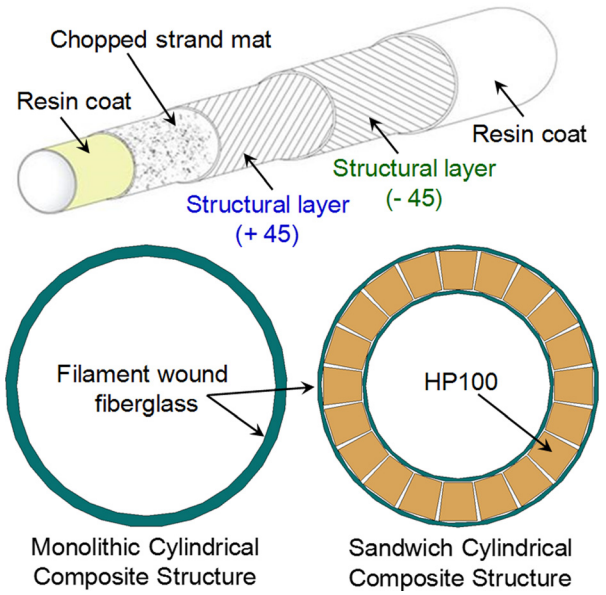

Fig. 2 Components of thick-walled, small *L*/*D* cylindrical fiberglass structure with [45 deg/−45 deg] layup

structure is manufactured by cutting the PVC foam into the required segments, inserting into concentric composite cylinders and impregnating the assembly with polyester resin. The inside surfaces of the cylindrical specimens are painted with an enamel spray to improve reflectivity for high-speed photography.

The thin-walled, large *L*/*D* ratio specimens are carbon fiber reinforced composite cylinders arranged in a [±15 deg/0 deg/±45 deg/±15 deg] layup with a 380 mm length, 60 mm inner diameter, and 1.5 mm wall thickness. This dimension is selected to provide specimens with relatively low collapse pressure and a high diameter-to-thickness ratio so that the thin-wall assumptions could be applied [19–22]. The cylindrical specimen model is built with two aluminum caps sealed at the ends. Figure 3 shows the configuration and layup of the thin-walled, large *L*/*D* composite cylinder.

4 Numerical Framework

Finite element models accounting for large deformations, material damage, and FSI effects are developed in the present work. Linear orthotropic elastic constitutive behavior is adopted for the composite plies. Damage initiation and evolution for each ply are predicted based on the Hashin damage model [29,30]. The Deshpande and Fleck crushable foam plasticity model is used to describe the constitutive behavior of the PVC foams [31].

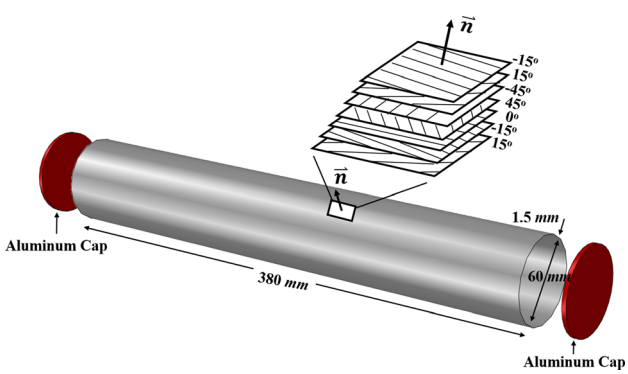

Fig. 3 Configuration and layup of thin-walled, large *L*/*D* composite cylinder

4.1 Cohesive Finite Element Framework. In the study case of thick-walled, small *L/D* structures, finite element simulations using the experimental conditions and independently measured material properties are conducted to support the experiments. The simulations account for the FSI effect at the water–composite interface, shear cracking and fragmentation in the core, matrix cracking and fiber failure in the faces, and core-face interfacial debonding. Both the bulk composite and PVC foam follow an isotropic linear elastic constitutive relation. Cohesive elements are specified between all the bulk element boundaries in the glass-reinforced polyester as well as PVC foam. The cohesive elements allow for damage initiation and development. For the zero-thickness cohesive elements, a bilinear cohesive law is adopted to govern traction–separation behavior. A schematic representation of the bilinear traction–separation law is shown in Fig. 4. Loading initially proceeds from point A to B, at which point softening occurs with increasing strain until failure at a separation of δ. Because it is not physically meaningful for compressive tractions to contribute to damage initiation, only tensile normal tractions are considered in the damage initiation rule. Once damage is initiated in a cohesive element, the interface follows the mixed-mode fracture criterion [32] (details about the CFEM approach presented here can be found in Refs. [33–36]). After failure of cohesive elements, contact between bulk elements leads to frictional sliding. The surfaces that are fractured are identified as potential contact regions and master and slave surfaces are assigned to the corresponding bulk element faces. When the surfaces come in contact with one another, the Coulomb friction law governs the interfacial frictional force. The coefficient of friction is 0.6, which is typical for composite sliding [37].

The CFEM models with cohesive traction–separation behavior with finite initial stiffness have two competing requirements on element size. The upper bound requires that the element size must be small enough to accurately resolve stress distribution inside cohesive zones at crack tips. The lower bound requires the cohesive surface induced stiffness reduction be minimal such that wave speed in the solid is not significantly affected. For the current analysis, the element size of 50 μm is calculated using the criteria specified in Ref. [35].

4.2 Coupled Eulerian Lagrangian Framework. In the study case of thin-walled, large *L/D* structures, finite element simulations based on the CEL approach through the nonlinear finite element commercial code, ABAQUS [30], are performed to characterize the dynamic response of structures subjected to combined loads of hydrostatic pressure and high-intensity impulsive loads. The specimen is sealed using two aluminum end caps. Boundary conditions are applied at one of the end caps to prevent translation in all the directions and rotations around all the three axes. Translation in the axial direction is allowed at the other end. Since the effects of hydrostatic pressure are of interest, the initial stress state in the structure is established in a static analysis. The structural state is then imported as the initial conditions in the dynamic analysis [18,19,38,39], where the Eulerian material (water) can interact with Lagrangian elements (cylindrical structure) through Eulerian–Lagrangian contact to allow fully coupled multiphysics FSI simulations. The initial static pressure is applied throughout the dynamic analysis procedure. Simulations are carried out with various combinations of hydrostatic and explosive loading. The upper bound of the hydrostatic pressure is determined through a linearized buckling analysis conducted using the software package [18,19,39], which is denoted as P_c, i.e., critical collapse pressure of the structure.

In the CEL framework, the cylinder is located within an Eulerian chamber which is used to generate a blast wave as shown in Fig. 5. A blast wave can be generated by specifying a chosen profile of velocity $v(t)$ at the inflow Eulerian boundary condition, and the blast wave $p(t)$ can be observed at some distance L downstream [40–42]. The input velocity profile is defined as [30]

$$v(t) = v_0 + v_p \exp\left[-(t - t_0)/t_d\right] \tag{1}$$

Here, v_0 is the initial particle velocity, v_p is the peak particle velocity, t_0 defines the start time, and t_d defines the duration of the blast velocity profile. A one-dimensional Eulerian model (one string of brick Eulerian elements) is used to calibrate the numerical blast waves as shown in Fig. 5(*a*). The first element at the inflow is subjected to a chosen particle velocity boundary condition $v(t)$, and the element at the assumed location of the specimen outputs the expected incident blast wave. Zero displacement boundary conditions are applied on the side of the model to restrict flow normal to the walls but allow tangential flow. The nonreflecting outflow Eulerian boundary condition is specified at the end of the model. Figure 5(*b*) presents the pressure profile for the blast wave recorded at different downstream locations with $v_0 = 0$, $v_p = 90$ mm/s, $t_0 = 2.8 \times 10^{-4}$ s, and $t_p = 10^{-5}$ s.

A very fine mesh is required to properly capture the instantaneous rise in overpressure. If the size of elements is too large, the peak of the overpressure will be rounded down and the rise time will be elongated. Figure 5(*c*) shows the results of the mesh refinement study. It is evident that an Eulerian element with size of 1 mm would suffice for the purpose.

The response of water in the Eulerian domain is described by the Mie–Grüneisen equation of state such that

$$p = \frac{\rho_0 c_0^2 \eta}{(1 - s\eta)^2}\left(1 - \frac{\Gamma_0 \eta}{2}\right) + \Gamma_0 \rho_0 E_m \tag{2}$$

where p is the pressure, c_0 is the speed of sound, ρ_0 is the initial density, E_m is internal energy per unit mass, Γ_0 is Grüneisen's gamma at a reference state, $s = dU_s/dU_p$ is the Hugoniot slope coefficient, U_s is the shock wave velocity, and U_p is the particle velocity which is related to U_s through a linear Hugoniot relation

$$U_S = c_0 + sU_p \tag{3}$$

The parameters for the Mie–Grüneisen equation of state are listed in Table 1.

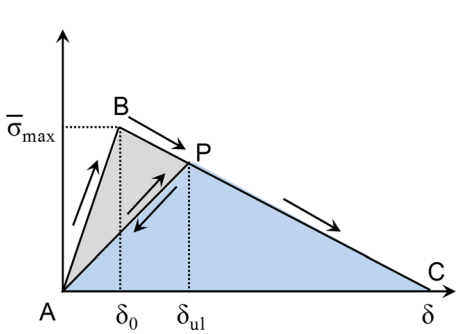

Fig. 4 Bilinear traction–separation law for cohesive elements

5 Results, Analysis, and Discussion

5.1 Thick-Walled Structures With Small *L/D*. In this combined experimental and computational study, the materials of choice are glass fiber reinforced polymer and structural PVC foam, commonly found in marine construction. According to the experimental investigation, structural attributes, loading intensities, and constituent properties determine the overall damage response through the activation of different failure mechanisms. In response to the impulsive loads specified in Fig. 1(*b*), a stress wave propagates through the curved composite laminate. The stress wave propagation is initially perpendicular to incident wave and follows the curvature of the cylindrical structure. Figure 6

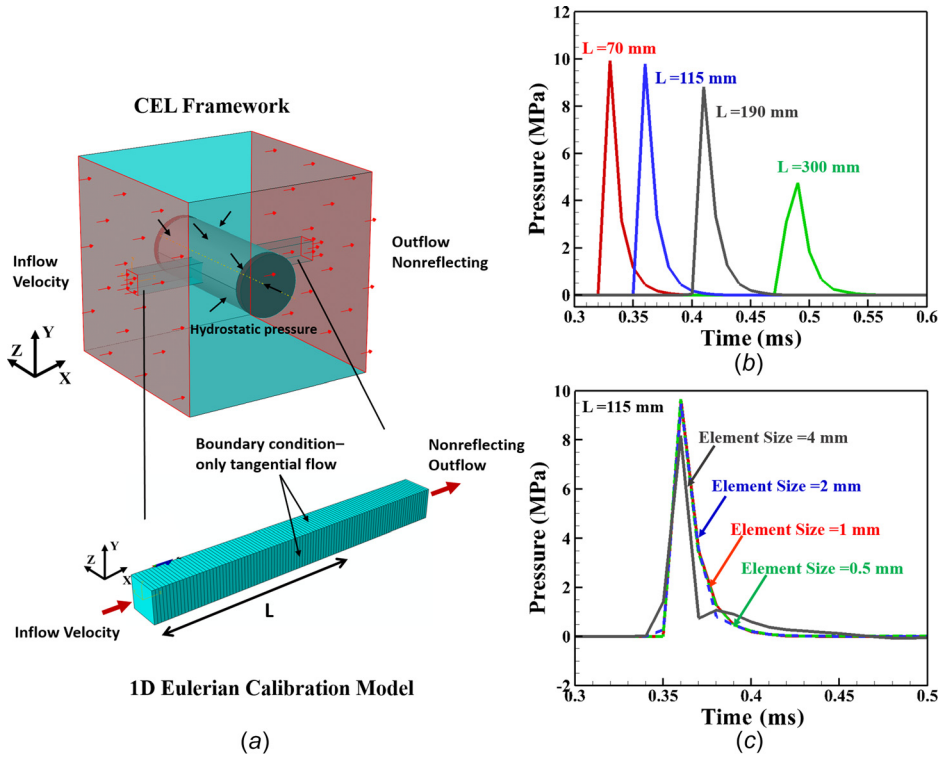

Fig. 5 (*a*) Schematic illustration showing the CEL framework for studying the implosion event, (*b*) output pressure profile at different downstream locations within the Eulerian domain, and (*c*) Eulerian mesh sensitivity studies showing the output pressure profile at $L = 115$ mm

Table 1 Parameters for the Mie–Gruneisen equation of state for water

ρ_0 (kg/m^3)	c_0 (m/s)	Γ_0 (dimensionless)	$s = dU_s/dU_p$ (dimensionless)
980	1500	0.1	1.75

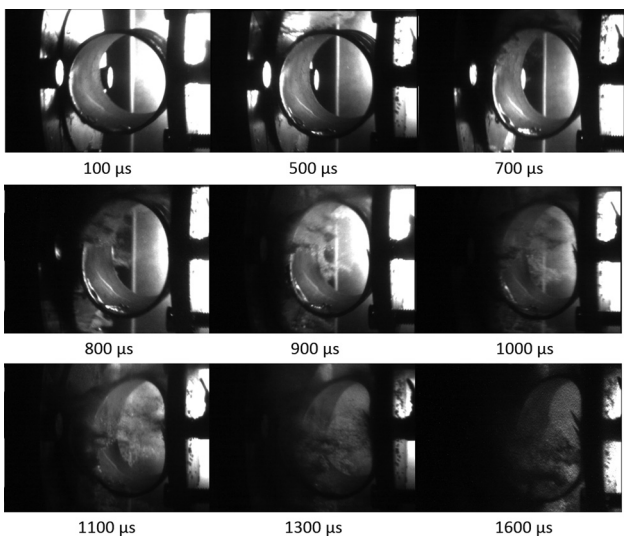

Fig. 6 High-speed photographs of a monolithic composite structure subjected to an impulsive load generated by a projectile velocity of $V_0 = 50$ m/s

shows the high-speed photographs of a monolithic composite cylinder subjected to an underwater impulsive load corresponding to a projectile velocity of 50 m/s. The high-speed photographs capture the dynamic deformation and warping in the composite cylinder. Visual inspection of post-test specimens reveals that four types of damage modes are observed in both monolithic and sandwich structures: (1) delamination, (2) matrix cracking and fiber rupture, (3) structural warping, and (4) core compression and partial recovery. Results from the numerical analysis of the response of cylindrical structures to localized blasts provide insight and a more in-depth understanding of the failure modes, progressive damage, and energy dissipation. As in experiments, a planar underwater impulsive wave is incident on the side of the cylinder simulating a "side-on" loading condition in the CFEM framework.

Figure 7 shows the stress wave propagation with a sequence of magnified images of damage initiation and evolution in the cylindrical monolithic composite structure. As the stress wave propagates through the composite structure, the bonds between successive laminates fail and delamination occurs at $t = 200\,\mu$s. When the interlaminar crack jumps from one interface to another, it inevitably leads to matrix cracking and intralaminar crack growth. Due to the dynamic nature of this process, buckling initiates in the composite structure and causes cracking and failure in the laminates as observed at $t = 600\,\mu$s. As deformation progresses, the intralaminar cracks link together to create a shear band along which the entire laminate undergoes failure and rupture.

Figure 8 shows the stress wave propagation with a sequence of magnified images of damage initiation and evolution in the cylindrical sandwich composite structure. Initially, the stress wave travels through the outer face, creating highly stressed regions at the core-outer face interface. The core undergoes significant compression and minor cracking. Although large-scale delamination is caused due to the incident loads, intralaminar cracking does not

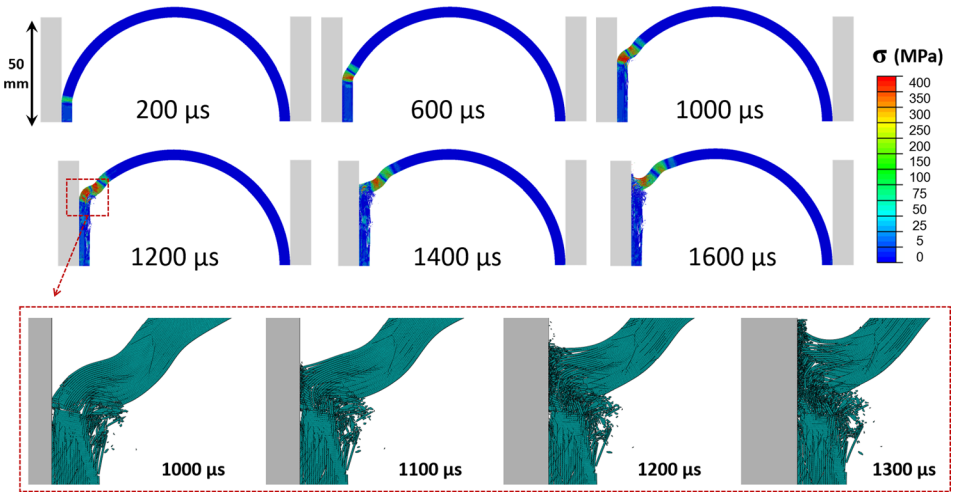

Fig. 7 Stress wave propagation in a cylindrical monolithic composite structure at different times with magnified images showing damage initiation and evolution

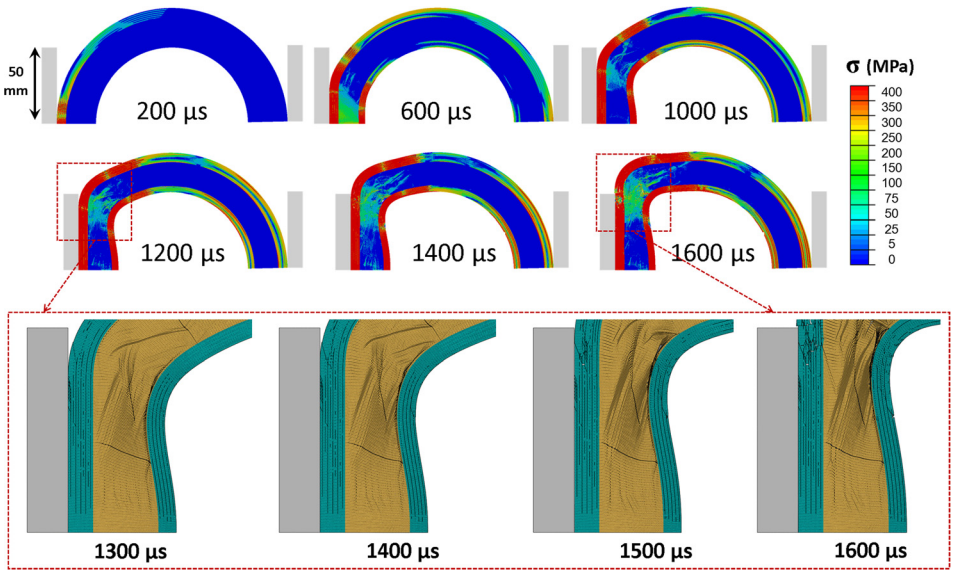

Fig. 8 Stress wave propagation in a cylindrical sandwich composite structure at different times with magnified images showing damage initiation and evolution

initiate. Due to the absence of intralaminar cracking, there is no structural rupture in spite of the reduction in overall strength due to delamination. This indicates that in addition to improve the overall stiffness of the cylindrical structure, the PVC foam core also improves blast mitigation by alleviating some of the effects of flexural wave propagation in the composite sections. For similar incident impulsive loads, sandwich composites outperform monolithic composite.

Figure 9 shows a comparison of energy dissipation in the form of fracture, friction, and elastic deformation. Results indicate that for a similar applied impulse, the sandwich structure dissipates almost twice as much energy as the monolithic structure. This is primarily because of the presence of a compressible foam core and a thinner outer face, which contribute to higher elastic strain and fracture work, respectively.

Overall, filament-wound cylindrical structures exhibited good resiliency under blast loading. While the monolithic structure showed signs of severe internal damage and warpage, the sandwich structure was relatively unwarped and recovered most of the original geometry.

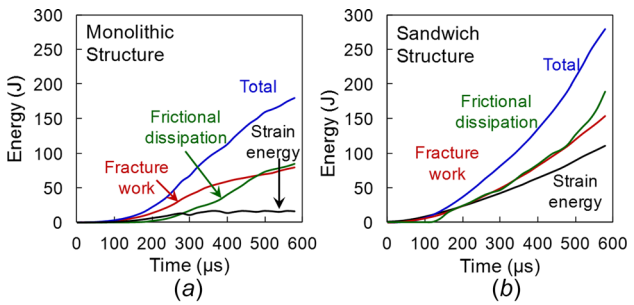

Fig. 9 Total energy dissipation in (*a*) monolithic and (*b*) sandwich structures subjected to similar impulsive loads

5.2 Thin-Walled Structures With Large *L*/*D*. In this computational study, the choice of material is carbon fiber reinforced composite, in relation to the latest experimental work on explosive-induced implosion of composite tubes [20]. The analyses focus on the effect of varying loading configurations on

structural collapse and damage. Time = 0 s indicates the start of the dynamic procedure.

5.2.1 Effect of Orientation of the Impulsive Loading. The cylindrical structure is loaded in two different cases separately as shown in Fig. 10(*a*), i.e., a side-on shock wave propagating perpendicular to the axis of the cylinder (case 1) and a side-on shock wave propagating parallel to the axis of the cylinder (case 2). Loads are generated using the framework described in Sec. 4.2 to mimic the high-pressure, exponentially decaying impulses. The higher load is applied in case 2 because the structure is stiffer in the axial direction. A constant uniform pressure with the magnitude of $0.8P_c$ is applied to the cylinder surface throughout the analysis procedure.

Figure 11 compares the contact pressure measured at four different locations about the midspan of the cylinder for the two loading cases, i.e., location A at the left of the cylinder (closest to the explosive source in case 1), location B in the upper part of the cylinder, location C in the lower part of the cylinder, and location D at the right of the cylinder (farthest to the explosive source in case 1). In case 1, features of pressure history vary with locations. There is a delay among the peak pressures measured at the different locations. Based on the pressure profile and the simulation snapshots of the deformation of the structure, shown in Fig. 11(*a*), the collapse event in case 1 can be described in the following three stages:

(1) From the beginning of the initial shock wave until ~0.6 ms, higher impulse experienced at the left of the cylinder dominates the structural deformation. The left wall moves faster and the structure undergoes an asymmetric shape collapse, which is verified by the simulation snapshot in Fig. 11(*a*).
(2) During 0.6–0.8 ms, the impulse applied to the structure is reduced all around the cylinder. The highly compressed structure starts to relax based on the asymmetric mode shape.
(3) After ~0.8 ms, various shock wave experienced all around the cylinder is "modifying" the collapse shape of the structure. The opposing walls of the cylinder start to contact each other due to the higher impulse experienced at the right of the cylinder. The wall contact indicates the initiation of the implosion event studied by researchers [19–22].

In comparison, contact pressure measured in case 2, as shown in Fig. 11(*b*), shows similar features at different locations about the midspan. This leads to the symmetric collapse mode shape, which is verified by the simulation snapshots in Fig. 11(*b*).

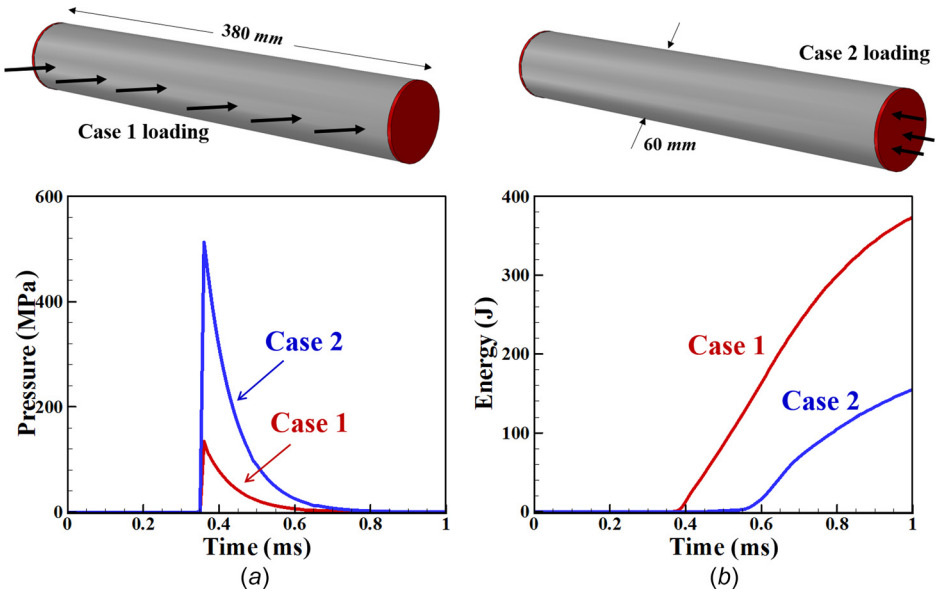

Fig. 10 (*a*) Initial shock for cases 1 and 2 loading conditions and (*b*) damage dissipation energy for the two loading cases

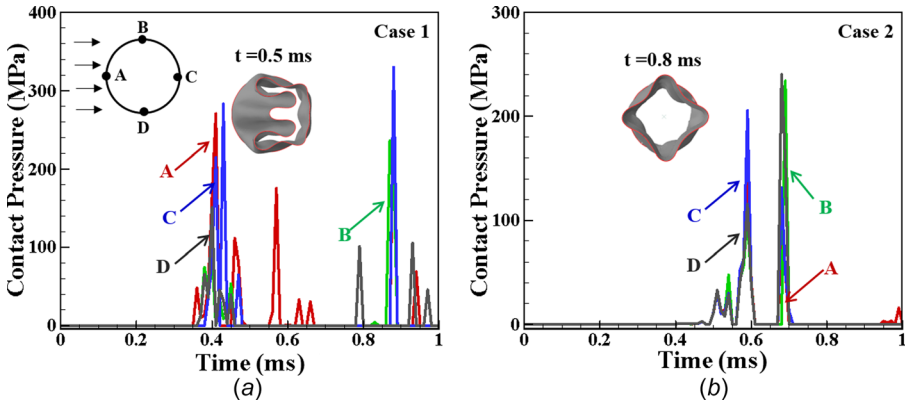

Fig. 11 Contact pressure profiles measured at different locations about the midspan of the cylinder for (*a*) case 1 loading condition and (*b*) case 2 loading condition

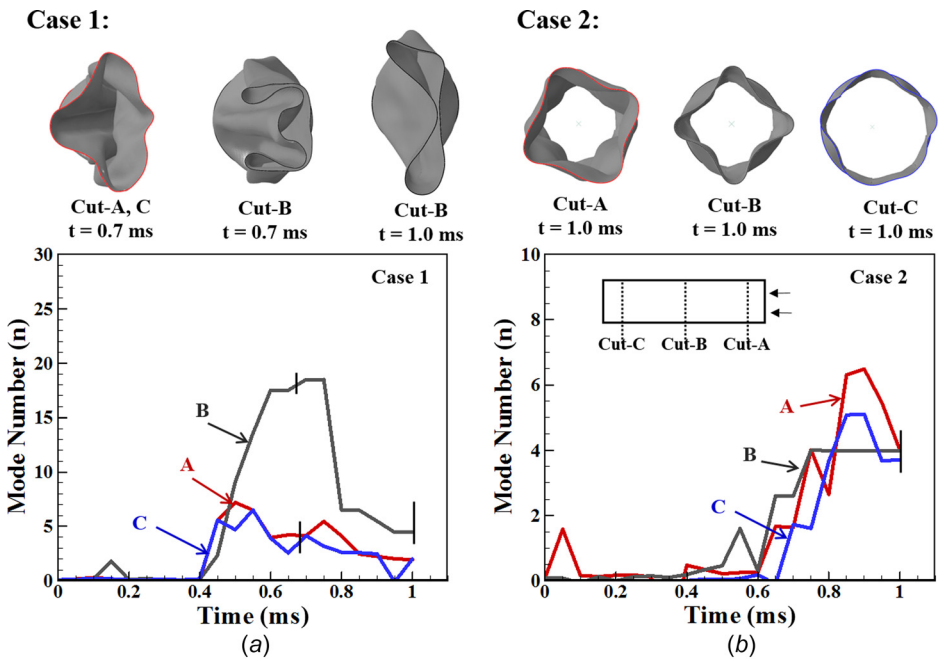

Fig. 12 Collapse mode shape evolution at different axial locations of the cylinder for (*a*) case 1 loading condition and (*b*) case 2 loading condition

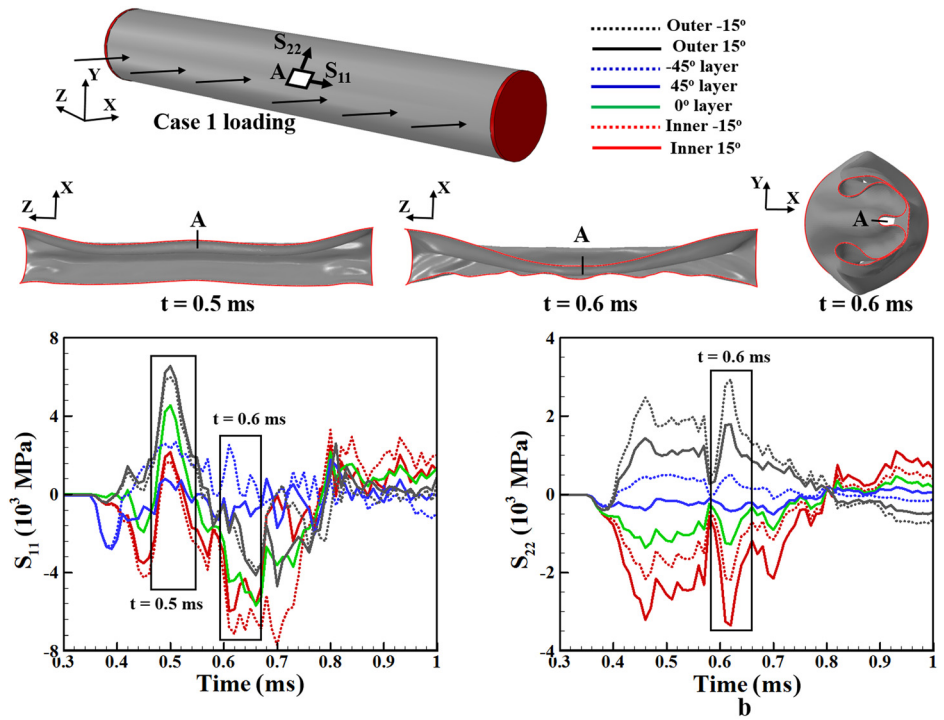

Fig. 13 Histories of stress at each ply in the laminated composite associated with structural deformation: (*a*) axial stress and (*b*) hoop stress

To further examine the collapse mode shape evolution, a Fourier series is used to represent the radial displacement of the cylinder at a certain axial location as a function of angular position [1,22]

$$u_R = a + b\cos(n\theta) + c\sin(n\theta) \tag{4}$$

Here, θ represents the angular position, a, b, c, and n are the fitting parameters, and n is the collapse mode number. Equation (4) is fit to the displacement profile at each time step of the dynamic procedure to obtain the mode number, n, and the value is plotted versus time. This study is performed at three different axial locations of the cylinder, i.e., location A near the right end of the cylinder (closer to the explosive source in case 2), location B which is the midspan of the cylinder, and location C (symmetric to location A about the midspan), for two different loading cases. In case 1, the predicted mode number is extremely high which may not be the real situation since the structure is highly compressed and exhibits

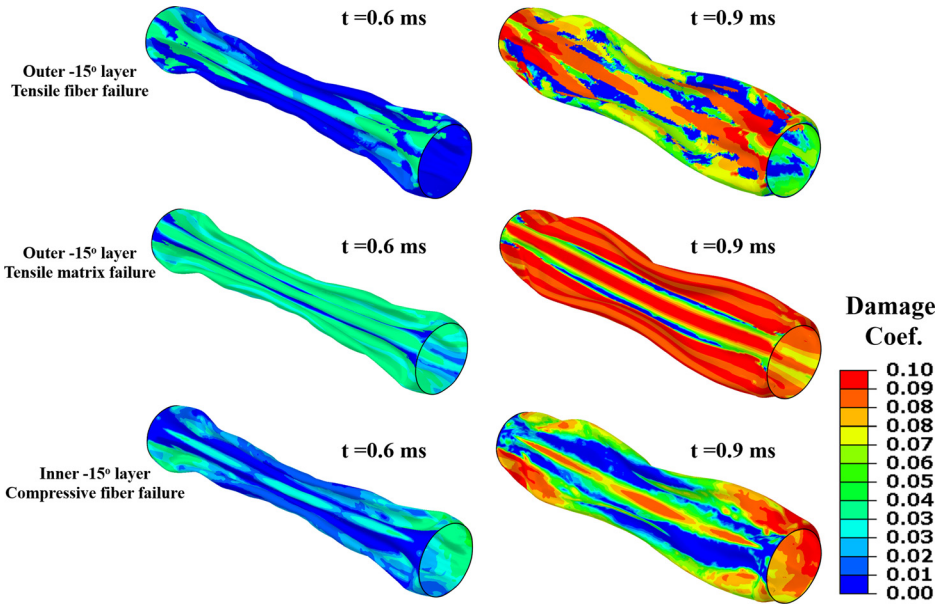

Fig. 14 Progressive damage evolution with different modes for the typical inner and outer plies in the laminated composite

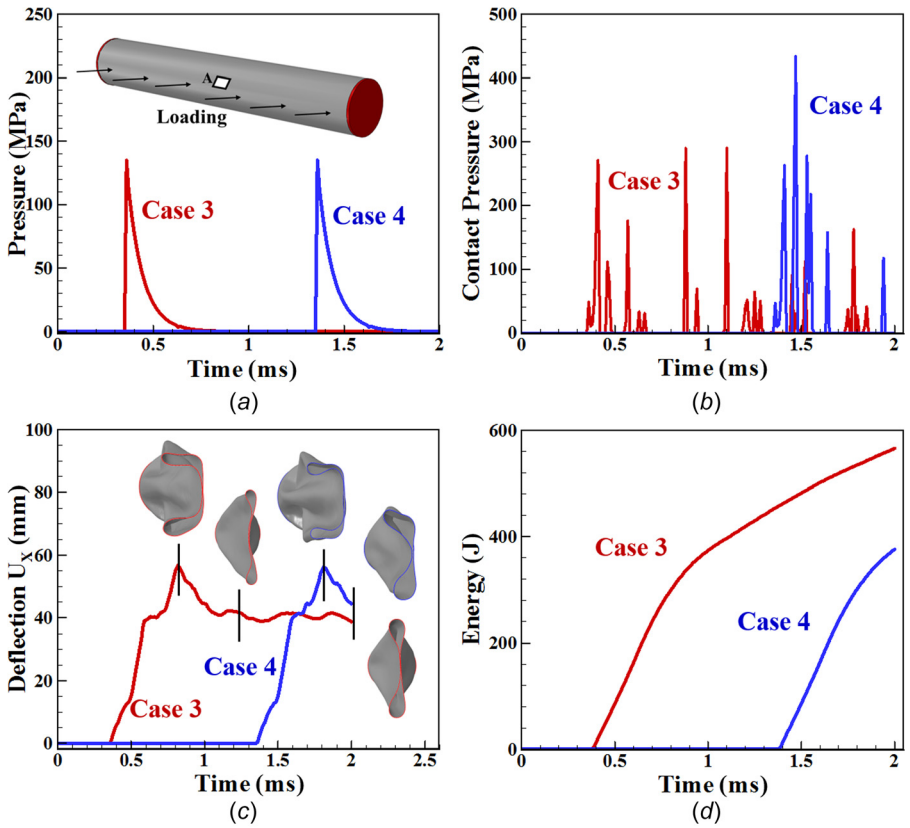

Fig. 15 (*a*) Initial shock for cases 3 and 4, (*b*) contact pressure profiles measured at location A about the midspan of the cylinder for cases 3 and 4, (*c*) deflections measured at point A about the midspan of the cylinder for cases 3 and 4, and (*d*) damage dissipation energy for cases 3 and 4

asymmetric collapse modes, as shown in Fig. 12(*a*). However, the evolution of the mode number, i.e., increasing sharply during the first stage and decreasing sharply at the end of the second stage, agrees with the previous discussion about the collapse event and the results from earlier studies on implosion [1,22]. Due to the decay of the initial shock wave, the cylinder tends to flatten in a perfect mode 2 shape as predicted [19–22], shown in Fig. 12(*a*). This deformation at the midspan is propagating along the length

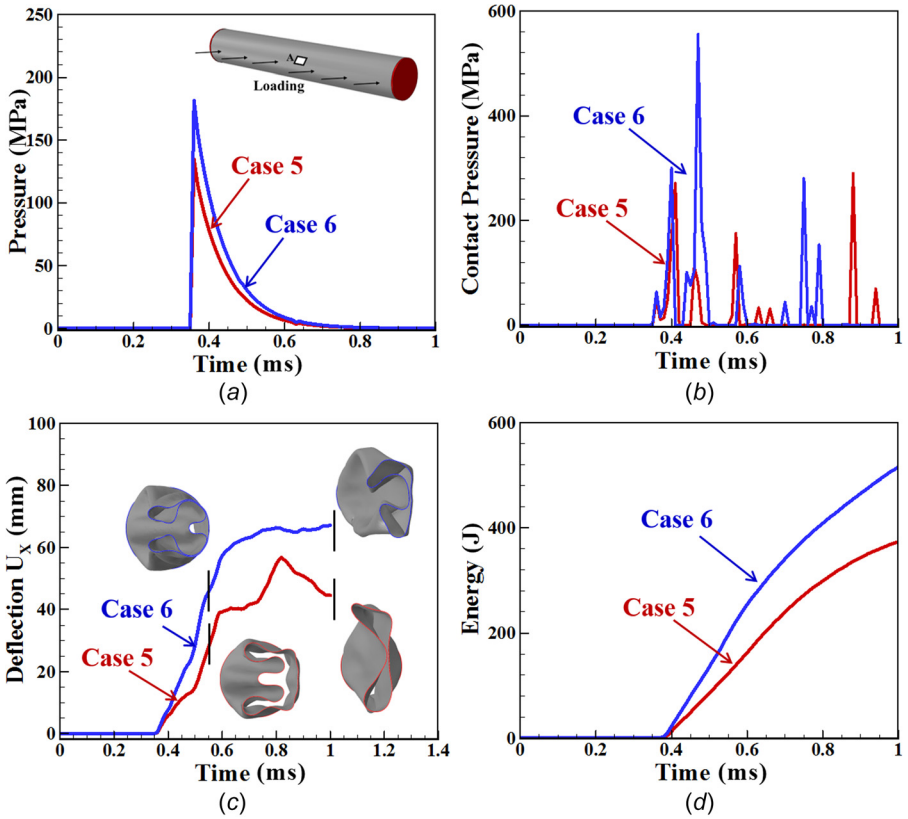

Fig. 16 (*a*) Initial shock for cases 5 and 6, (*b*) contact pressure profile measured at location A about the midspan of the cylinder for cases 5 and 6, (*c*) deflection measured at point A about the midspan of the cylinder for cases 5 and 6, and (*d*) damage dissipation energy for cases 5 and 6

to the ends of the cylinder (locations A and C). The evolution of the mode number at the locations near the ends exhibits similar features, and the predicted numbers agree well with the deformation obtained from the simulation. In case 2, the mode number at the three locations varies with time in almost the same trend. Due to shock wave variations discussed previously, the structure tends to exhibits a symmetric collapse mode, which is predicted as mode ~4, shown in Fig. 12(*b*).

To further explore the structural deformation and material damage in case 1, the layup stress at the left on the midspan of the cylinder (location A, closest to the explosive source in case 1) is plotted in Fig. 13. The stresses of interest are axial stress, S_{11}, and hoop stress, S_{22}. The variation of the axial stress is associated with the bending in axial direction, and the variation of the hoop stress is associated with the bending in circumferential direction. The deformation of the structure with corresponding to the stress state is shown in Figs. 13(*a*) and 13(*b*). For example, the collapse mode shape shown in Fig. 13(*b*) requires the bending in the circumferential direction at point A. This leads to the higher tensile stress in outer plies and higher compressive stress in inner plies, both of which are represented as the hoop stress in the structure.

The stress state discussed above further affects the damage evolution in the composite layup. Based on the plot in Fig. 13, outer plies undergo larger axial stress which leads to the severe tensile fiber failure, and larger hoop stress which leads to the severe tensile matrix failure. Inner plies experience larger hoop stress (negative), which accelerates the evolution of the compressive fiber damage. The progressive damage evolution of different plies with the current deformation states of the structure is shown in Fig. 14. These failure modes initiate and further form a band-shape damage or a longitudinal crack at the front wall (the face subjected to the initial shock) of the cylinder. This effectively reduces the stiffness of the structure and results in the rapid acceleration of the contact of the opposing walls of the cylinder to exhibit a mode 2 collapse shape.

Figure 10(*b*) shows a comparison of the damage dissipation energy in cases 1 and 2. The structure is more resistant to case 2 loading. Under case 1 loading, the structure collapses in higher mode shapes, severe damage initiates and accumulates at the cylinder wall, which leads to higher dissipated energy.

5.2.2 Further Analysis of Case 1 Loading. Explosion-initiated implosion is affected by factors such as initial shock, hydrostatic pressure, bubble pulse, and loading time (accumulation of damage) [17,20,39]. To explore the effect of loading time, case 1 loading is applied to the structure at different times separately to mimic the situation of explosion occurring at different times. The initial shock with the same intensity and decay time is shown in Fig. 15(*a*). In case 3, the impulsive loading is applied at an earlier time (~0.3 ms), and in case 4, the impulsive loading is applied at a later time (~1.3 ms). Both are loaded for 2 ms, and a constant uniform pressure with the magnitude of $0.8P_c$ is applied to the cylinder surface throughout the analysis. Figures 15(*b*)–15(*d*) compare the contact pressure, deflection, and damage dissipation energy for the two different cases. The contact pressure is measured at the left, on the midspan of the cylinder (location A, closest to the explosive source). The deflection (U_X) is measured as the displacement at location A. Case 4 has a higher shock pressure, however, in case 3, multiple bubble pulse pressure loadings are initiated following the initial shock wave. This leads to the accumulation of damage throughout the process and higher energy dissipated in case 3. By examination of the deflection and the deformation snapshots shown in Fig. 15(*c*), we conclude that the structural deformation history for the two cases follows similar patterns induced by the initial shock wave. However, there is a delay in the deformation state of case 4, since the explosion

occurs at a later time. The collapse is settling to mode 2 shape eventually during the implosion event as discussed earlier for both cases.

To mimic the effects of different amounts and stand-off distances of the explosion sources, impulsive loading with different intensities is applied to the structure. Uniform pressure of different magnitudes is applied to the cylinder surface throughout the analysis to explore the effect of the combinations. The initial shock profile is shown in Fig. 16(*a*). In case 5, a combination of lower impulsive loading and higher hydrostatic pressure ($0.8P_c$) is applied. In case 6, a combination of higher impulsive loading and lower hydrostatic pressure ($0.4P_c$) is applied. Figures 16(*b*)–16(*d*) compare the contact pressure, deflection, and damage dissipation energy for the two different cases. The contact pressure is measured at the left on the midspan of the cylinder (location A, closest to the explosive source). The deflection (U_X) is measured as the displacement at location A. The impulsive loading applied in the two cases is large enough compared to the hydrostatic pressure. Both structures undergo asymmetric collapse with high mode numbers, as shown in Fig. 16(*c*). The structure tends to settle to a mode 2 shape in both cases. Severe hoop stress is developed at the front wall due to circumferential bending. It suggests that one may rearrange the layup or line the cylinder with a flexible coating at certain angular positions to prevent the development of longitudinal cracks.

6 Conclusions

The response of thick-walled and thin-walled composite cylindrical structures subjected to underwater impulsive loads is investigated experimentally and computationally. The following observations are made:

(1) Experiments show that monolithic and sandwich composite structures exhibit multiple competing failure modes including core compression, delamination, core-face debonding, translaminar cracking, and matrix and fiber rupture. For similar total mass, the sandwich structure provided considerably superior blast mitigation as compared to the monolithic composite structure.

(2) The cohesive finite element model provides a unique approach to track the different damage modes in curved composites. Although the numerical model captures the essential deformation mechanisms, it slightly overestimates the effects of matrix cracking and rupture. Therefore, the cohesive element properties need to be recalibrated to ensure accurate representation of experimentally observed failure characteristics. Additionally, the rate-dependent behavior of the core material of sandwich structures is an important aspect that needs to be investigated.

(3) The numerical results for the thin-walled structure using the coupled Eulerian Lagrangian framework provide an insight into the deformation mechanisms and energy dissipation in the composite structures during the implosion event. Results show that the structure is more failure-resistant under axial loading than side-on loading. The stress analysis on the ply level provides an insight into the stress–structural deformation–damage evolution relationship during the severe explosion-induced implosion event.

(4) Explosion-induced implosion of composite cylinders is affected by different factors, such as the initial shock, the dynamic pressure created by the surrounding fluid, hydrostatic pressure, and loading time (damage accumulation). The phenomenon of collapse depends both on the geometry of the structure as well as the composite material lay-up, ply thickness, and properties. The numerical capability can be utilized to design and optimize composite structures under the extreme loading conditions with the account of above factors. This topic will be further pursued in future work.

(5) The current study provides design recommendations for improving the ability of composite cylinders to mitigate the effects of dynamic loading. For monolithic composites, filament-wound specimens are shown to provide the best resistance to damage. Tailoring the fiber orientation of facesheets, lining the cylinder with a flexible coating, and initially pressurizing the cylinder internally are effective measures for improving the design of composite cylinders. Compared with monolithic composites, sandwich structures with compressible foam cores have superior blast-resistance. Blast-mitigation is relatively insensitive to facesheet properties and highly sensitive to core properties. High-density cores lead to high transmitted impulse and high overall damage. Low-density cores experience high compressive strains and lead to lower transmitted impulse. Increased core compression is detrimental to bending stiffness and strength. Structural design must balance the competing requirements.

Acknowledgment

The authors gratefully acknowledge the support by the Office of Naval Research (Program Manager: Dr. Yapa D. S. Rajapakse).

References

[1] Fatt, M. S. H., and Pothula, S. G., 2010, "Dynamic Pulse Buckling of Composite Shells Subjected to External Blast," Compos. Struct., **92**(7), pp. 1716–1727.
[2] Gning, P., Tarfaoui, M., Collombet, F., and Davies, P., 2005, "Prediction of Damage in Composite Cylinders After Impact," J. Compos. Mater., **39**(10), pp. 917–928.
[3] Gning, P., Tarfaoui, M., Collombet, F., Riou, L., and Davies, P., 2005, "Damage Development in Thick Composite Tubes Under Impact Loading and Influence on Implosion Pressure: Experimental Observations," Composites, Part B, **36**(4), pp. 306–318.
[4] Tarfaoui, M., Gning, P.-B., and Collombet, F., 2007, "Residual Strength of Damaged Glass/Epoxy Tubular Structures," J. Compos. Mater., **41**(18), pp. 2165–2182.
[5] Tarfaoui, M., Gning, P.-B., Davies, P., and Collombet, F., 2007, "Scale and Size Effects on Dynamic Response and Damage of Glass/Epoxy Tubular Structures," J. Compos. Mater., **41**(5), pp. 547–558.
[6] Hernandez-Moreno, H., Douchin, B., Collombet, F., Choqueuse, D., and Davies, P., 2008, "Influence of Winding Pattern on the Mechanical Behavior of Filament Wound Composite Cylinders Under External Pressure," Compos. Sci. Technol., **68**(3–4), pp. 1015–1024.
[7] Tarfaoui, M., Gning, P. B., and Hamitouche, L., 2008, "Dynamic Response and Damage Modeling of Glass/Epoxy Tubular Structures: Numerical Investigation," Composites, Part A, **39**(1), pp. 1–12.
[8] Avachat, S., and Zhou, M., 2010, "Dynamic Response of Submerged Composite Sandwich Structures to Blast Loading," IMPLAST 2010—SEM Fall Conference, Arun Shukla, ed., Providence, RI, Oct. 12–14.
[9] Avachat, S., and Zhou, M., 2011, "Dynamic Response of Composite Sandwich Structures Subjected to Underwater Impulsive Loads: Experiments and Simulations," 16th International Conference on Composite Structures, ICCS-16, A. J. M. Ferreira, ed., FEUP, Porto, Portugal.
[10] Avachat, S., and Zhou, M., 2011, "Effect of Facesheet Thickness on Dynamic Response of Composite Sandwich Plates to Underwater Impulsive Loading," Exp. Mech., **52**(1), pp. 83–93.
[11] Avachat, S., and Zhou, M., 2016, "Compressive Response of Sandwich Plates to Water-Based Impulsive Loading," Int. J. Impact Eng., **93**, pp. 196–210.
[12] Dannemann, K., Chalivendra, V., and Song, B., 2012, "Dynamic Behavior of Materials," Exp. Mech., **52**(2), pp. 117–118.
[13] Espinosa, H. D., Lee, S., and Moldovan, N., 2006, "A Novel Fluid Structure Interaction Experiment to Investigate Deformation of Structural Elements Subjected to Impulsive Loading," Exp. Mech., **46**(6), pp. 805–824.
[14] Latourte, F., Gregoire, D., Zenkert, D., Wei, X., and Espinosa, H. D., 2011, "Failure Mechanisms in Composite Panels Subjected to Underwater Impulsive Loads," J. Mech. Phys. Solids, **59**(8), pp. 1623–1646.
[15] McShane, G., Stewart, C., Aronson, M., Wadley, H., Fleck, N., and Deshpande, V., 2008, "Dynamic Rupture of Polymer–Metal Bilayer Plates," Int. J. Solids Struct., **45**(16), pp. 4407–4426.
[16] Avachat, S., and Zhou, M., 2014, "Response of Cylindrical Composite Structures to Underwater Impulsive Loading," Proc. Eng., **88**, pp. 69–76.
[17] Gish, L., 2015, "Designing Implodable Underwater Systems to Minimize Implosion Pulse Severity," OCEANS'15 MTS/IEEE, IEEE, Washington, DC, Oct. 19–22.
[18] Leduc, M., 2011, "On the Implosion of Underwater Composite Shells," Master's thesis, The University of Texas at Austin, Austin, TX.
[19] Pinto, M., Gupta, S., and Shukla, A., 2015, "Study of Implosion of Carbon/Epoxy Composite Hollow Cylinders Using 3-D Digital Image Correlation," Compos. Struct., **119**, pp. 272–286.

[20] Pinto, M., and Shukla, A., 2015, "Shock-Initiated Buckling of Carbon/Epoxy Composite Tubes at Sub-Critical Pressures," Exp. Mech., **56**(4), pp. 1–12.
[21] Pinto, M., and Shukla, A., 2016, "Mitigation of Pressure Pulses From Implosion of Hollow Composite Cylinders," J. Compos. Mater., **50**(26), pp. 3709–3718.
[22] Pinto, M., and Shukla, A., 2015, "Dynamic Collapse Mode Evolution in Carbon Composite Tubes," Extreme Mech. Lett., **3**, pp. 55–58.
[23] Turner, S. E., and Ambrico, J. M., 2013, "Underwater Implosion of Cylindrical Metal Tubes," ASME J. Appl. Mech., **80**(1), p. 011013.
[24] Farhat, C., Wang, K., Main, A., Kyriakides, S., Lee, L.-H., Ravi-Chandar, K., and Belytschko, T., 2013, "Dynamic Implosion of Underwater Cylindrical Shells: Experiments and Computations," Int. J. Solids Struct., **50**(19), pp. 2943–2961.
[25] Gupta, S., LeBlanc, J. M., and Shukla, A., 2014, "Mechanics of the Implosion of Cylindrical Shells in a Confining Tube," Int. J. Solids Struct., **51**(23–24), pp. 3996–4014.
[26] Gupta, S., LeBlanc, J. M., and Shukla, A., 2015, "Implosion of Longitudinally Off-Centered Cylindrical Volumes in a Confining Environment," ASME J. Appl. Mech., **82**(5), p. 051002.
[27] McCoy, R., and Sun, C., 1997, "Fluid-Structure Interaction Analysis of a Thick-Section Composite Cylinder Subjected to Underwater Blast Loading," Compos. Struct., **37**(1), pp. 45–55.
[28] Diab, 2016, "Divinycell HP: High Temperature Resistant Core Suitable for Prepreg Applications," Diab Americas LP, DeSoto, TX, available at:, http://www.diabgroup.com/en-GB/Products-and-services/Core-Material/Divinycell-HP
[29] Hashin, Z., 1980, "Failure Criteria for Unidirectional Fiber Composites," ASME J. Appl. Mech., **47**(2), pp. 329–334.
[30] Hibbit, Karlsson, and Sorensen, 2009, "Abaqus/Explicit User's Manual, Version 6.9," Hibbit, Karlsson, and Sorensen, Inc., Providence, RI.
[31] Deshpande, V., and Fleck, N., 2001, "Multi-Axial Yield Behaviour of Polymer Foams," Acta Mater., **49**(10), pp. 1859–1866.
[32] Kenane, M., and Benzeggagh, M., 2009, "Characterization of Mixed Mode Delamination Growth and Thresholds," *Damage Fracture Mechanics*, Springer, New York, pp. 523–530.
[33] Minnaar, K., and Zhou, M., 2004, "A Novel Technique for Time-Resolved Detection and Tracking of Interfacial and Matrix Fracture in Layered Materials," J. Mech. Phys. Solids, **52**(12), pp. 2771–2799.
[34] Zhai, J., Tomar, V., and Zhou, M., 2004, "Micromechanical Simulation of Dynamic Fracture Using the Cohesive Finite Element Method," J. Eng. Mater. Technol., **126**(2), pp. 179–191.
[35] Tomar, V., Zhai, J., and Zhou, M., 2004, "Bounds for Element Size in a Variable Stiffness Cohesive Finite Element Model," Int. J. Numer. Methods Eng., **61**(11), pp. 1894–1920.
[36] Qu, T., Prakash, C., and Tomar, V., 2016, "Relating Interface Properties With Crack Propagation in Composite Laminates," Int. J. Chem. Mol. Nucl. Mater. Metall. Eng., **3**(6), pp. 665–668.
[37] Schön, J., 2000, "Coefficient of Friction of Composite Delamination Surfaces," Wear, **237**(1), pp. 77–89.
[38] Yin, C., Jin, Z., Chen, Y., and Hua, H., 2016, "Shock Mitigation Effects of Cellular Cladding on Submersible Hull Subjected to Deep Underwater Explosion," Ocean Eng., **117**, pp. 221–237.
[39] Gish, L. A., 2013, "Analytic and Numerical Study of Underwater Implosion," Ph.D. thesis, Massachusetts Institute of Technology, Cambridge, MA.
[40] Mougeotte, C., Carlucci, P., Recchia, S., and Ji, H., 2010, "Novel Approach to Conducting Blast Load Analyses Using Abaqus/Explicit-CEL," Army Armament Research Development and Engineering Center, Picatinny Arsenal, NJ.
[41] Chen, A., Louca, L. A., and Elghazouli, A. Y., 2016, "Behaviour of Cylindrical Steel Drums Under Blast Loading Conditions," Int. J. Impact Eng., **88**, pp. 39–53.
[42] Chen, A., Louca, L. A., and Elghazouli, A. Y., 2015, "Blast Assessment of Steel Switch Boxes Under Detonation Loading Scenarios," Int. J. Impact Eng., **78**, pp. 51–63.